

# Predicting sit-to-stand adaptations due to muscle strength deficits and assistance trajectories to complement them

Vinay Kumar<sup>1,\*</sup>, Takahide Yoshiike<sup>2</sup>, and Tomohiro Shibata<sup>1,\*</sup>

<sup>1</sup>Department of Human Intelligence Systems, Graduate School of Life Science and Systems Engineering, Kyushu Institute of Technology, Kitakyushu, Japan

<sup>2</sup>Honda R&D Co., Ltd., Saitama, Japan

Correspondence\*:

Vinay Kumar  
vinaym815@gmail.com

Tomohiro Shibata

tom@brain.kyutech.ac.jp

## 2 ABSTRACT

3

4 Sit-to-stand (STS) transition is the most bio-mechanically challenging task necessary for  
 5 performing activities of daily life. With muscle strength being the most dominant, many co-  
 6 occurring factors influence how individuals perform STS. This study investigates the changes in  
 7 STS caused by muscle strength deficits and how they might lead to unsuccessful STS. It also  
 8 presents the external assistance trajectories that can complement strength deficits for successful  
 9 STS transition. Towards these aims, first, the STS trajectories generated for musculoskeletal  
 10 models with different strength deficits using single shooting optimization are presented. The  
 11 muscle strength deficits were introduced by simultaneously scaling the maximum isometric  
 12 strength of muscles in steps of 20%. The optimization could generate successful STS transition  
 13 for the 0%, 20%, and 40% strength deficit models. The common activation patterns among these  
 14 trajectories agree with the literature for all the muscles except the rectus femoris. Comparison  
 15 of these trajectories shows that the STS duration increases with strength deficits while the  
 16 peak vertical center of mass velocity and the peak gluteus maximus and vastus muscle forces  
 17 decrease. Also, with strength deficits, the hamstring muscle activation reduces, which relieves the  
 18 antagonistic vastus muscle but stresses the agonistic gluteus maximus muscle. Subsequently, the  
 19 vastus muscle weakness is proposed to cause unsuccessful STS transition of the 60% strength  
 20 deficit model using motion tracking results. Finally, the successful STS trajectory generated  
 21 for the 60% strength deficit model assisted externally at the torso is presented. The trajectory  
 22 features utilization of external assistance as and when needed to complement strength deficits for  
 23 successful STS transition. Our results will help plan intervention and design novel STS assistance  
 24 devices.

25 **Keywords:** Sit-To-Stand, Musculoskeletal Model, Strength Deficit, Single Shooting Optimization, Open Loop Controller, Assist-A-  
 26 Needed

## 1 INTRODUCTION

27 Sit-to-stand (STS) transition is a precursor to walking, hence critical for performing daily life activities and  
 28 an independent lifestyle. Lower extremity strength plays an important role in human STS, and its deficits

are thought to limit the STS functionality. Studies have shown that the lower extremity strength is a strong predictor of the ability to perform STS from the lowest chair height for older adults (Hughes et al., 1996; Schenckman et al., 1996). However, the decline in muscle strength often co-occurs with other physiological and psychological impediments such as reduced balance, joint pain, and depression, making it difficult to access its independent effect on STS using experiments (Lord et al., 2002). Also, besides subject-specific factors, STS is influenced by many extrinsic factors like foot placement, knee position, and chair height, which makes the designing of experiments complex.

Some past studies have used STS trajectories generated using optimization and musculoskeletal models to avoid the complications of experiments (Pandy et al., 1995; Bobbert et al., 2016; Yokota et al., 2016). Pandy et al. (1995) presented a cost function that generates STS trajectories with similar muscle activations to those of experiments. Bobbert et al. (2016) and Yokota et al. (2016) searched for trajectories that reduced loads on the muscles and the knee joint. However, these studies have made either minimal or no observations about STS changes caused by strength deficits. Further, these studies have not investigated how strength deficits might lead to unsuccessful STS.

Many older individuals incapable of independent STS transition can perform the same when aided externally. When provided in an assist-as-needed manner, this external assistance can help maintain or recover lower extremity strength. Thus it is desirable to generate reference assistance trajectories that assist as and when needed and by the amount needed for successful STS transition. Mombaur and Hoang (2017) and Geravand et al. (2017) have used optimization to discover assistance trajectories that support part of the user's weight during STS and squat-to-stand motions, respectively. However, both the studies use human models with independently torque actuated joints. The hamstrings and the rectus femoris are two biarticular muscles that play an essential role in the STS transition. Their biarticularity couples the torques produced at the hip and knee joints. This coupling should not be ignored, especially when generating STS assistance trajectories, as it may lead to over actuation of one of these muscles, leading to muscle contracture and eventually lower back issues. The coupling is also crucial for the proper investigation of the STS changes and the STS failure caused by the strength deficits.

This study aims to identify the changes in STS caused by muscle strength deficits, investigate how they might lead to unsuccessful STS transition, and generate the external assistance trajectories that can complement muscle strength deficits for successful STS transition. Towards these aims, we first systematically generated STS trajectories for musculoskeletal models with varying degrees of strength deficit using single shooting optimization. Then we contrasted these trajectories against literature for validation and against each other to observe the changes in STS caused by strength deficits. Subsequently, motion-tracking was used to investigate how strength deficit might lead a musculoskeletal model to unsuccessful STS transition. Finally, STS trajectories were generated for a musculoskeletal model incapable of performing unaided STS transition when assisted externally at the torso. The findings of this study will help plan intervention and design novel STS assistance devices that operate in an assist-as-needed manner.

It is not easy to identify and detail all of the parameters that shape the STS trajectories generated using optimization. For example, Bobbert et al. (2016), and Yokota et al. (2016) does not contain information about the initial guesses to the optimization algorithm, while Pandy et al. (1995) does not include information about the mechanical limits used to restrict the motion to the physiologically plausible range. Therefore we will make all the source code and results from this study public at <https://github.com/ShibataLab/PredictiveSTS>.

## 2 METHODS

An overview of the single shooting optimization framework used to solve the dynamic optimization problem of generating STS simulations in this study is shown in Figure 2. The optimization framework tunes the values of decision variables using the aCMA-ES algorithm (Arnold and Hansen, 2010). aCMA-ES is a stochastic gradient-free optimization algorithm that adapts a Gaussian distribution towards low energy regions and was selected for its enhanced robustness to the locally optimal solution compared to the gradient-based algorithms. At each generation, aCMA-ES samples a batch of candidate solutions from the Gaussian distribution being adapted. Subsequently, the cost function values are computed for all the candidates by running forward simulations. aCMA-ES then adapts the Gaussian distribution based on the cost function values and proceeds to the next generation and so on until one of the stopping criteria is met. The following subsections detail the different components of the optimization framework and the motion-tracking setup used to investigate STS failure.

### 2.1 Musculoskeletal Model

Musculoskeletal models with different strength deficits for this study were obtained by simultaneously scaling the maximum isometric strengths of the muscles present within the base model. The base model, also shown in Figure 1, is a simplified version of the LaiArnold2017 model (Lai et al., 2017). The LaiArnold2017 model represents an average-sized adult male of mass 75 kg and height 170 cm. The base model is two-dimensional with eight hill-type muscles and three degrees of freedom. The simplifications were needed to make the optimization problem computationally tractable. The following paragraph detail some of these simplifications.

From the LaiArnold2017 model, the left leg was removed while the mass and inertia of the right foot were doubled. The masses of arms, forearms, and hands were lumped to the torso's center of mass (COM). The right foot was fixed to the ground using a weld joint. Then the degrees of freedom corresponding to the motion of the ankle, knee, and hip joints in the sagittal plane were added (Figure 1 **B**). The  $0^\circ$  angle of the hip, knee, and ankle joints corresponds model standing upright. From  $0^\circ$ , the positive joint angles correspond to ankle dorsiflexion, knee flexion, and hip flexion; and negative joint angles correspond to the opposite. The lower extremity muscles with similar functions from the LaiArnold2017 model were combined to single muscle-tendon units as is realized in Ong et al. (2019). The maximum isometric strengths of the right leg muscles were doubled to account for the missing left leg muscles. Figure 1 shows the eight hill-type muscles included in the base model, i.e., gluteus maximus, hamstrings, iliopsoas, rectus femoris, vastus, gastrocnemius, soleus, and tibialis anterior. Table 1 lists the acronyms of these muscles and their maximum isometric strengths for the base model.

The chair-body contact interactions were modeled using a kinematic constraint between the femur and the chair. The kinematic constraint was disabled during simulation when the vertical reaction forces required to maintain it turned non-compressive. The model has nonlinear torsional springs representing ligaments at hip, knee, and ankle joints to limit the motion to a physiologically plausible range. They generate torques when the hip joint flex beyond  $120^\circ$  or extends below  $30^\circ$ , or the knee joint flex beyond  $140^\circ$  or extend beyond  $0^\circ$ , or the ankle dorsiflex beyond  $30^\circ$  or plantarflex beyond  $40^\circ$ .

External assistance was introduced at the torso's COM in the musculoskeletal model that failed to perform unaided STS transition. The rationale behind introducing it at the torso is explained in subsection 3.3. The external assistance was modeled using two independent point forces acting in the vertical and horizontal directions. Their respective magnitudes were limited to the 0-400 N range. The excitation signals to point forces were passed through first-order activation dynamics before computing actuation.

113 The first-order activation dynamics (Millard, 1999) is the same as those of the hill-type muscle present  
 114 within the musculoskeletal models and had a time constant of 0.1 sec. It made the assistance trajectories  
 115 smoother and thus helped the optimization algorithm. The OpenSim API (Delp et al., 2007) was used to  
 116 formulate the musculoskeletal model's equation of motion and their forward integration.

## 117 2.2 Simulation Setup

118 The STS simulation was divided into two phases. During the first phase, the kinematic constraint between  
 119 the femur and chair plane, representing the chair-body contact interactions, was active, while during the  
 120 second phase, it was not. The kinematic constraint was disabled during simulation when the vertical  
 121 reaction forces required to maintain it turned non-compressive. Once disabled, the kinematic constraint  
 122 could not be re-engaged, i.e., the simulation could only transition from the first phase to the second one  
 123 and not vice-versa. The two-phase simulation division prevented optimization from getting stuck into  
 124 local optima with multiple chair rises. At the beginning of the simulation, the muscle states were set  
 125 by equilibrating the muscle and tendon forces with the muscle activations prescribed by the excitation  
 126 trajectories. The upper limit of simulation duration was fixed to 1.6 seconds, as this is approximately the  
 127 time a young adult takes to stand up. The simulation was terminated before 1.6 sec if the model approached  
 128 the condition of being upright represented in Equation 1.

$$|\theta_{hip}| + |\theta_{knee}| + |\theta_{ankle}| \leq 10^\circ \quad (1)$$

## 129 2.3 Optimization Setup

130 Our optimization framework tuned the values of nodes points obtained by discretizing the excitation  
 131 trajectories of the actuators present within the musculoskeletal model, i.e., muscles and external assistance.  
 132 Piecewise linear functions were used for this discretization. The time difference between the consecutive  
 133 node points had a fixed value of 0.1 sec. The upper limit of simulation duration was 1.6 sec. All the  
 134 musculoskeletal models had 8 hill-type muscles. The externally assisted musculoskeletal model had  
 135 additional actuators, i.e., 2 point force representing the external assistance. Thus, the optimization problem  
 136 had 136 decision variables when generating unaided STS trajectories and 170 decision variables when  
 137 generating assisted STS trajectories.

138 The excitation values corresponding to the model sitting in the chair were used as the initial guess to  
 139 the aCMA-ES. A standard deviation of 0.3 was used as the initial guess for each decision variable to the  
 140 optimization algorithm. A population size of 90 was used for each generation. The optimization algorithm  
 141 was stopped if the number of generations exceeded 7000 or if the improvement in the cost function value  
 142 of the best candidate solution in the last 250 generations was less than 0.5 . We used the *libcmaes* library  
 143 (CMA-ES, 2013) for the aCMA-ES algorithm.

## 144 2.4 Cost Function

145 The cost function we selected to engender STS transition is a linear combination of ten different terms  
 146 and can be expressed as follows:

$$\phi_{total} = \sum_{i=1}^{10} w_i C_i \quad (2)$$

147 where  $w_i$  is the relative weight of  $i^{th}$  cost term, i.e.,  $C_i$ . The  $w_i$  values were determined heuristically and  
 148 are listed in Table 2. The mathematical expressions for the ten cost terms are given in eqs. 3 - 13. Please  
 149 refer to Table 3 for the list of symbols used in these equations.

$$C_1 = \int_{t_0}^{t_f} \exp(t|\tau_{boundary}) [y_{com}(t_0) - y_{com}(t)] dt \quad (3)$$

$$C_2 = \int_{t_0}^{t_f} \exp(t|\tau_{boundary}) |x_{talus}(t_0) - x_{com}(t)| dt \quad (4)$$

$$C_3 = \int_{t_0}^{t_f} \exp(t|\tau_{chair}) F_{chair,y}(t) dt \quad (5)$$

$$C_4 = \sqrt{\frac{\sum_m \int_{t_0}^{t_f} a_m(t)^2 dt}{\sum m}} \quad (6)$$

$$C_5 = \sqrt{\frac{\sum_m \int_{t_0}^{t_f} \dot{a}_m(t)^2 dt}{\sum m}} \quad (7)$$

$$C_6 = \int_{t_0}^{t_f} ||F_{Assist}(t)|| dt \quad (8)$$

$$C_7 = \sum_n \int_{t_0}^{t_f} |T_{n,limit}(t)| dt \quad (9)$$

$$C_8 = \int_{t_0}^{t_f} \left( \text{bool}(|F_{feet,x}(t)| > \mu|F_{feet,y}(t)|) \times (|F_{feet,x}(t)| - \mu|F_{feet,y}(t)|) + \text{bool}(|F_{chair,x}(t)| > \mu|F_{chair,y}(t)|) \times (|F_{chair,x}(t)| - \mu|F_{chair,y}(t)|) \right) dt \quad (10)$$

$$C_9 = \int_{t_0}^{t_f} |ZMP_x(t) - x_{talus}(t_0)| dt \quad (11)$$

$$C_{10} = \int_{t_0}^{t_f} - \left( \text{bool}(F_{heel,y}(t) < 0) \times F_{heel,y}(t) + \text{bool}(F_{toe,y}(t) < 0) \times F_{toe,y}(t) \right) dt \quad (12)$$

$$\exp(t|\tau) = \frac{e^{t/\tau}}{\tau[e^{t_f/\tau} - 1]} \quad (13)$$

150 Costs  $C_1$  and  $C_2$  leads the optimization to standing posture. Cost  $C_3$  encourages the transition of  
 151 simulation from the first phase to the second. Cost  $C_4$  corresponds to control effort exerted by the muscles  
 152 during STS. Cost  $C_5$  ensures that the muscles are activated or deactivated smoothly. Cost  $C_6$  corresponds to  
 153 external assistance effort. This term was equal to be zero for the STS trajectories of unaided musculoskeletal  
 154 models. Cost  $C_7$  penalizes hyper-flexion and hyper-extension of joints. Cost  $C_8$  penalizes contact forces  
 155 that would lead to slip if the bodies were not constrained. Cost  $C_9$  penalizes feet contact forces that would  
 156 lead to tipping over the toes or heel. Cost  $C_{10}$  penalizes feet contact forces that are non-compressive.

157 Costs  $C_1$  to  $C_3$  use an exponential scaling function, i.e.,  $\exp()$ , expressed in Equation 13. As shown in  
 158 Figure 3, the  $\exp()$  function gives higher weightage to values observed later in the simulation. Its behavior  
 159 is defined entirely by the time constant  $\tau$ . We used the value of  $t_f/24$ , also referred to as  $\tau_{boundary}$ , for the  
 160 time constants of terms  $C_1$  and  $C_2$ , and of  $t_f/3$ , also referred to as  $\tau_{chair}$ , for the cost term  $C_3$ . Figure 3  
 161 shows the graphs of  $\exp(t|\tau_{boundary})$  and  $\exp(t|\tau_{chair})$  for  $t_f = 1.6\text{sec}$ . The area under the  $\exp()$  curve  
 162 between 0 to  $t_f$  is equal to one. The  $\exp()$  function spreads the rewards over a longer duration and makes it  
 163 easier for the optimization framework to obtain rewards.

164 The ten cost terms can be divided into three categories. The first category leads the optimization to  
 165 standing posture and consists of costs  $C_1$  to  $C_3$ . The second category penalizes the effort exerted and  
 166 consists of costs  $C_4$  to  $C_6$ . Costs  $C_7$  to  $C_{10}$  belong to the third category representing the constraints the  
 167 optimized trajectory should respect. Using an optimization framework that supports non-linear trajectory  
 168 constraints, like direct collocation (Bobbert et al., 2016), would have required only the costs from the  
 169 second category. All the remaining terms would have been modeled as non-linear trajectory constraints  
 170 in such a framework. However, due to its simplicity and ease of future extension to incorporate feedback  
 171 control loops, we decided to use the single shooting optimization framework.

## 172 2.5 Motion Tracking Setup

173 The OpenSim CMC tool-based motion tracking was used to investigate the failure of STS in this study.  
 174 The CMC tool computes the actuator excitation levels at user-specified time intervals that will drive the  
 175 generalized coordinates ( $\vec{q}$ ) of the musculoskeletal model towards a desired kinematic trajectory ( $\vec{q}_{\text{exp}}$ ) in  
 176 the presence of external forces. At any given time  $t$ , the CMC tool first computes the desired acceleration  
 177  $\ddot{\vec{q}}^*$  using the following proportional derivative control law:

$$178 \quad \ddot{\vec{q}}^*(t+T) = \ddot{\vec{q}}_{\text{exp}}(t+T) + \vec{k}_v \left[ \dot{\vec{q}}_{\text{exp}}(t) - \dot{\vec{q}}(t) \right] + \vec{k}_p [\vec{q}_{\text{exp}}(t) - \vec{q}(t)] \quad (14)$$

178 where,  $\vec{k}_v$  and  $\vec{k}_p$  are the feedback gains on the velocity and position errors, respectively. Since the  
 179 forces that muscles apply cannot change instantaneously, the desired accelerations are computed some  
 180 small-time  $T$  in the future. Then, CMC tool uses static optimization to distribute the load across synergistic  
 181 actuators using static optimization. CMC tool offers two formulations for static optimization referred to as  
 182 slow target and fast target. We used the fast target formulation. It minimizes the sum of squared controls  
 183 augmented by a set of equality constraints which can be mathematically represented as follows:

$$J = \sum_{i=1} e_i^2 \quad (15)$$

$$C_j = \ddot{q}_j^* - \ddot{q}_j \quad \forall j \quad (16)$$

184 where  $e_i$  is the control input/excitation of  $i^{th}$  actuator at time  $t$  and  $q_j$  is the  $j^{th}$  generalized coordinate.  
 185 Since for many  $\ddot{q}_j^*$  the muscles might not be able to produce sufficient forces, usually ideal torque actuators  
 186 are added to the musculoskeletal model to prevent the fast target formulation from failing. Usually, the  
 187 forces/torques produced per unit control effort for the ideal actuators is much lower than muscles. In  
 188 such setups, following equation 15, ideal torque actuators produce significant force/torque only when the  
 189 muscles are saturated, and hence they are also referred to as reserve actuators. Since the CMC tool does not  
 190 support event detection based disabling of constraints, the seat contact force was supplied as an external

191 force rather than a kinematic constraint. The seat force was pre-computed for the target STS trajectory  
 192 before running the CMC tool.

### 3 RESULTS

193 The strength deficits were increased in steps of 20% to obtain the different musculoskeletal models. For  
 194 each musculoskeletal model, three independent optimization runs were used to obtain three different locally  
 195 optimal solutions. Out of the three, only the STS trajectory corresponding to the optimal solution with  
 196 the lowest cost (Equation 2) is reported here. The optimization could generate successful STS trajectories  
 197 for the 0%, 20%, and 40% strength deficit models. However, for the 60% strength deficit model, the  
 198 optimization framework could only generate a successful STS trajectory when the model was assisted  
 199 externally at the torso. For conciseness, we refer to these trajectories as those of the models even though  
 200 the models were only one component of the complete optimization framework.

201 The STS trajectories are divided into four phases as suggested in Millington et al. (1992) to facilitate  
 202 discussions. Figure 4 shows these four kinematics-based phases for the STS trajectory of the 0% strength  
 203 deficit model. Phase 1 starts with the trunk flexion and ends when the knee extension starts. Phase 2 starts  
 204 with the knee extension and ends when the hip joint is maximally flexed. Phase 3 begins with the reversal  
 205 of trunk flexion to extension and ends with the model standing upright. Mathematically the end of phase 3  
 206 is defined as the time when the horizontal velocity of the COM becomes zero. Phase 4 is the balancing  
 207 phase, and during it, the model sways back and forth while standing. We have not any observations about  
 208 the features of phase 4 in this study as the STS transition is complete at the end of phase 3. The dotted  
 209 black lines in Figures 4-6 marks the transition between the four phases.

210 The results are organized into three subsections. In subsection 3.1 first, the common patterns among the  
 211 unaided STS trajectories are reported and contrasted against literature for validation. Then, the adaptations  
 212 caused by muscle strength deficits are reported. Subsequently, in subsection 3.2, an explanation for the  
 213 failure of optimization to generate STS using the 60% strength deficit model is proposed. Finally, in  
 214 subsection 3.3, the features of the STS trajectory generated using the externally assisted 60% strength  
 215 deficit model are discussed. Please refer to Figures 4-6 and Table 4 during the following subsections for  
 216 details. The resultant joint torques, the muscle forces, and the contribution of muscle forces to resultant  
 217 joint torques in Figure 6 and Table 4 corresponds to the summation of respective values for right and left  
 218 legs. The resultant joint torques were obtained using inverse dynamical analysis of the STS trajectories  
 219 using OpenSimDelp et al. (2007). During inverse dynamical analysis, the forces produced by muscles were  
 220 excluded, while those of seat constraint and assistance were included as external forces. The contributions  
 221 of muscle forces to the resultant joint torques were computed using the Muscle Analysis tool of OpenSim.

#### 222 3.1 Unaided STS: Common Patterns and STS Adaptations

223 For all the unaided trajectories (Figure 6), the STS transition is initiated by activating the ILPSO muscle.  
 224 ILPSO activation generates torque around the hip joint and flexes the torso forward. It is followed by the  
 225 deactivation of ILPSO muscle and gradually increasing activations of the GMAX and HAMS muscles. The  
 226 GMAX and HAMS muscles undergo eccentric contraction to control the torso's forward flexion. As the  
 227 end of Phase 1 approaches, the activation of VAS muscle is increased to prepare for seat-off. Phase 1 ends  
 228 when the VAS muscle has generated sufficient torques around the knee joint to lift the musculoskeletal  
 229 model off the chair. During phase 2, the activation of GMAX, HAMS, and VAS muscles continues to  
 230 increase. The GMAX and HAMS activation reduces the hip flexion velocity until it becomes zero. At this  
 231 point, the trunk is maximally flexed, phase 2 comes to an end. The knee joint extends only slightly during  
 232 phase 2. During phase 3, the activation of GMAX, HAMS, and VAS muscles first increases, then peaks,

and finally tapers off. These patterns lead to the extension of both the hip and knee joints until the standing posture is achieved. The tapering off of the GMAX, HAMS, and VAS muscle activations during the latter half of phase 3 occurs because smaller forces are required to continue standing up since an increasing fraction of body weight is borne by bone alignment. At the end of phase 3, both the ILPSO and GAS are activated to stop the hip and knee joints from extending past the upright posture. Significant TA muscle activations are present during phase 1, phase 2, and the first half of phase 3. These activations produce the force needed to balance the counteracting SOL and GAS muscle forces. The SOL and RF muscles see almost negligible activation throughout the three phases. During phase 3, as the ankle plantarflexes, the passive fiber forces of the SOL muscle reduce. The peak GMAX, HAMS, and VAS muscle forces, as well as the peak hip and knee extension torques, occur during the first half of phase 3 (Figure 6). As the moment arms for muscles change with joint angles (Sherman et al., 2013), the peak forces and the peak contributions to resultant joint torques usually do not coincide (Figure 6). For example, during phase 3, the VAS muscle's peak contribution to resultant knee torque occurs later than the peak force. Because of the increased moment arm, the VAS muscle is able to generate peak contribution to resultant joint torque with reduced muscle force.

The general activation patterns of GMAX, HAMS, VAS, SOL, GAS, and TA muscles match those experimentally observed in Caruthers et al. (2016); however, those of RF muscle does not. Caruthers et al. (2016) reports significant activations of RF muscle from phase 1 to the first half of phase 3, while our trajectories feature only minimal activation of RF muscle during the same. Our trajectories feature significant activation of VAS muscle during the first half of phase 1, while Caruthers et al. (2016) reports minimal activation during the same time. Caruthers et al. (2016) does not report activations for ILPSO muscle.

The activation patterns of VAS, GMAX, HAMS, and SOL muscles observed in this study are similar to those from the generated STS trajectories of Pandy et al. (1995), and Bobbert et al. (2016). The GAS muscle activation patterns between this and Pandy et al. (1995) are also similar while Bobbert et al. (2016) does not report the same. Both Pandy et al. (1995) and Bobbert et al. (2016) observe significant RF activation before seat-off while our STS trajectories feature negligible RF activation throughout STS transition. Pandy et al. (1995) also observes higher RF activation at the beginning of motion. It was most likely because of the absence of ILPSO muscle in the musculoskeletal model used. Bobbert et al. (2016) does not report ILPSO activations. The variation TA muscle activation patterns between the three studies were most like because of the assumption of initial sitting posture.

With strength deficits, the STS duration increases, while the peak COM vertical velocity, peak GMAX, and VAS muscle forces and their respective contributions to peak resultant joint torques decrease (Table 4, Figure 6). With increasing strength deficits, the VAS muscle starts getting saturated first, followed by the GMAX muscles. The contribution of HAMS muscle to the peak resultant knee torques drops from -22.80%, -27.94% for the 0% and 20% strength deficit models to -12.91% for the 40% strength deficit model. While, the contribution of HAMS muscle to the peak resultant hip torques drops from 49.17%, 49.48% for the 0% and 20% strength deficit models to 37.14% for the 40% strength deficit model. The contribution of GMAX to peak resultant hip torques increased from 54.46%, 54.22% for the 0% and 20% strength deficit models to 64.58% for the 40% strength deficit model. Based on these percentages, it can be said that when the VAS muscle is not saturated, the HAMS muscle works with the GMAX muscle to control hip extension. When the VAS muscle starts getting saturated, the activation of HAMS muscle is reduced as it works opposite to VAS muscle along the knee joint. The reduced activation of HAMS muscle increases the stress on the GMAX muscle. Bobbert et al. (2016) also observes that with strength

277 deficits, the STS duration increases, while the peak COM vertical velocity, peak GMAX, and VAS muscle  
 278 forces decrease. However, Bobbert et al. (2016) does not observe a significant reduction in HAMS muscle  
 279 activation. This difference exists most likely because Bobbert et al. (2016) used the solution of the previous  
 280 optimal trajectory as the initial for the next optimization problem.

### 281 3.2 Failure to produce STS transition

282 The optimization framework failed to generate the STS transition for the 60% strength deficit model. We  
 283 suspected the GMAX or the VAS muscle to be responsible for this failure as they were getting saturated  
 284 during the STS trajectory of the 40% strength deficit model (Figure 6). The TA muscle was also getting  
 285 saturated; however, we did not inspect it since the TA muscle can easily be relieved by moving the feet  
 286 slightly forward. Moving the feet slightly forward will reduce the amount of ankle dorsiflexion and the  
 287 accompanying passive fiber forces of the counteracting SOL muscle.

288 We used the 60% strength deficit model and OpenSim CMC Tool to track the successful STS motion of  
 289 40Two different setups of reserve actuators were used to aid the muscles. In the first setup, the optimal  
 290 torque, i.e., torques generated per unit control effort, for the hip and knee torque actuators were  $100\text{Nm}$   
 291 and  $1\text{Nm}$  respectively, while in the second setup, they were  $1\text{Nm}$  and  $100\text{Nm}$ . The first setup favored  
 292 the utilization of the hip reserve actuator, while the second setup favored the utilization of the knee  
 293 reserve actuator. The motion-tracked using the first setup features a peak torque of  $-38.64\text{Nm}$  by the  
 294 knee reserve actuator and increased activation of both VAS and RF muscles. While the second setup-based  
 295 motion-tracking features a peak torque of only  $-3.66\text{Nm}$  by the hip reserve actuator and increased HAMS  
 296 and GMAX activations. The lower magnitude of reserve actuator in the second setup compared to the first  
 297 supports the hypothesis that the failure to generate STS motion for the 60% strength deficit model was  
 298 because of VAS muscle weakness. Also, the HAMS was not saturated during the STS motion of the 40%  
 299 strength deficit model (Figure 6) and could be actuated to assist GMAX if needed, further supporting the  
 300 hypothesis. Also, the magnitude of reserve actuators shows that it is possible to assist the model only at the  
 301 knee joint for successful STS transition without significant modification of motion.

### 302 3.3 Externally assisted STS transition

303 It was observed in the last subsection that assisting the musculoskeletal model primarily at the hip joint  
 304 leads to increased RF muscle activation while assisting it primarily at the knee joint leads to increased  
 305 HAMS muscle activation. As STS transition is performed several times a day, assisting only at the hip or  
 306 the knee joint will lead to the contracture of the RF or the HAMS muscle, respectively. As both the muscles  
 307 cross the hip joint in an antagonistic manner, their contracture has a high potential to lead to back pain  
 308 issues. Thus the external assistance was introduced at the torso COM in the 60% strength deficit model.  
 309 Also, assisting the model at the torso center of mass is a good approximation for assisting a human at the  
 310 underarms area. The underarms area is easily graspable, and assistance using it helps simplify the design of  
 311 a probable STS assistance device.

312 Physical assistance, when provided in an assist-as-needed manner, can help maintain or recover lower  
 313 extremity strength. Thus while generating the assisted STS trajectories, the over-utilization of external  
 314 assistance was penalized (Equation 8). Figure 5 shows the body postures and the assistance force trajectories  
 315 from the STS motion generated using the externally assisted 60% strength deficit model. The STS trajectory  
 316 features utilization of external assistance only when the VAS muscle starts getting saturated, i.e., it uses  
 317 external assistance only when needed. The peak magnitudes of the vertical and horizontal components of  
 318 external assistance are  $323.81\text{N}$  and  $77.53\text{N}$ , respectively. The external assistance is used to assist muscles  
 319 at both the hip and knee joints, as evidenced by the reduced peak resultant hip and knee joint torques (Table

320 4). The peak VAS, GMAX, and HAMS muscle forces are also lower than those from the STS motion of  
321 40% strength deficit models (Figure 6)).

## 4 DISCUSSION

322 This paper presented and analyzed the STS trajectories generated using open-loop single shooting  
323 optimization for musculoskeletal models with different muscle strength deficit levels. The strength deficits  
324 were introduced by scaling the maximum isometric strength of all the muscles in steps of 20%. The  
325 optimization could successfully generate STS trajectories for 0%, 20%, and 40% strength deficit models.  
326 The common muscle activation patterns reported in this study are in agreement with the literature, except  
327 for those of RF muscle. As muscle strength deficit increased, the peak VAS and GMAX forces, peak  
328 center of mass velocities reduced while the STS increased. When the VAS muscle started getting saturated  
329 (40% strength deficit model), the activation of the antagonistic HAMS muscle was reduced. The reduced  
330 HAMS muscle activation led to increased GMAX muscle activation. Then the motion-tracking results  
331 were used to propose the VAS muscle weakness as the reason for optimization's failure to generate an STS  
332 trajectory using the 60% strength deficit model. The motion tracking results were also used to motivate  
333 the introduction of external assistance at torso COM. Optimization was able to generate a successful STS  
334 trajectory for the externally assisted 60% strength deficit model. The trajectory featured lower peak GMAX,  
335 VAS, and HAMS muscle forces and the usage of external assistance in an assist-as-needed manner. We  
336 hope the results will help plan interventions and design novel STS assistance devices and thus have made  
337 all the source material public. However, the findings of this study should be observed with caution as it  
338 they have many inherent assumptions. The most significant among these known assumptions are discussed  
339 in the next paragraph.

340 Strength deficits were introduced by scaling the maximum isometric strength of all the muscles  
341 simultaneously. Bobbert et al. (2016) and Yokota et al. (2016) also introduced strength deficits in a  
342 similar manner. However, it might be the case that the strength of all muscles does not deteriorate by the  
343 same factor. Also, scaling the maximum isometric forces is not the only way to introduce strength deficits.  
344 For example, the peak muscle activations could have been limited to the same effect. Many studies have  
345 experimentally reported that the elderly flex their trunk much more than healthy young adults. Thus the  
346 elimination of lumbar joint, even though also made by Pandy et al. (1995), Bobbert et al. (2016), and Yokota  
347 et al. (2016), might be an oversimplification. During simulation, the model could not adjust its feet relative  
348 to the chair. It might have prevented the discovery of less demanding trajectories. Other musculoskeletal  
349 model-related critical assumptions are the sagittal plane of symmetry and simplification of muscle groups  
350 to single musculotendon units. No control level coupling between muscles was implemented, i.e., the  
351 muscles could be activated or deactivated independently; however, such might not be the case. The cost  
352 function used in this study is not unique in its capability to engender STS. Further, even for the selected  
353 cost function, the relative weights of the different cost terms should have been chosen using inverse optimal  
354 control. The relative weights were heuristically selected because of the computationally demanding nature  
355 of the optimization. The generated STS trajectories are local optimal solutions of nonlinear non-convex  
356 optimizations. The optimization's failure to generate STS using the 60% strength deficit model might have  
357 been because of the optimization setup rather than muscle saturation.

358 In the future, we plan to use the results of this study to design a kinematic events-based closed-loop  
359 controller for STS transition. We also plan to conduct experiments against whom the musculoskeletal  
360 model simplifications, and the generated STS trajectories can be verified. Finally, we intend to design an  
361 STS assistance device that operates on the assist-as-needed principle.

## 5 AUTHOR CONTRIBUTIONS

362 Conceptualization: VK, TY, and TS; Methodology: VK; Software: VK; Data Analysis: VK; Validation:  
363 TS; Writing—original draft preparation: VK; Writing—review and editing: VK, TY, and TS; Funding  
364 acquisition: TS; Resources: TY and TS; Supervision: TS

## 6 DATA AVAILABILITY STATEMENT

365 The optimization source code and the results from this study will be available <https://github.com/>  
366 ShibataLab/PredictiveSTS.

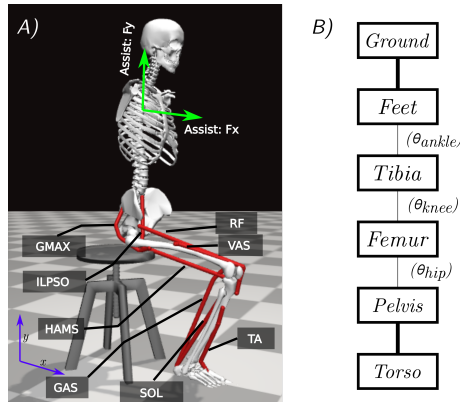


**Figure 1.** (A) The planar musculoskeletal model used for this study. The green arrows represent the horizontal and vertical component of external assistance force. (B) Degrees of freedom within the musculoskeletal model. Thick dark lines represent a weld joint.

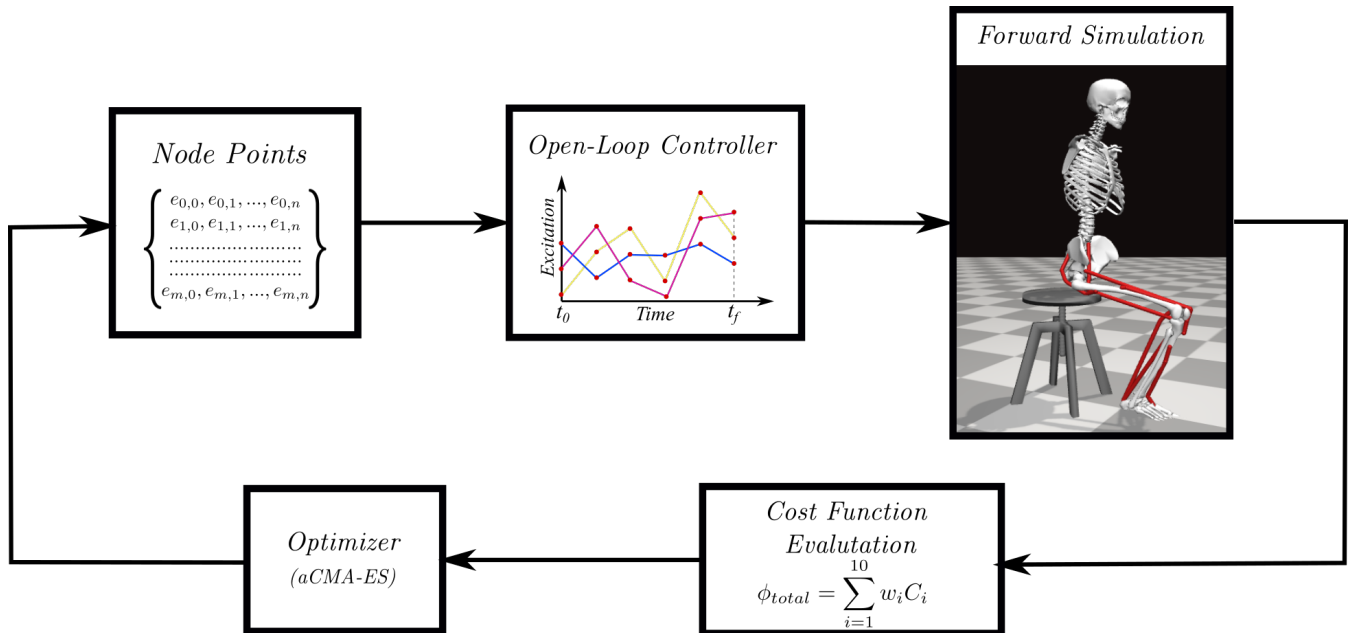


**Figure 2.** Overview of single shooting optimization framework. The red dots in the open-loop controller represents the node points obtained from the discretization of excitation trajectories.

Muscle	Acronym	Maximum Isometric Strength (N)
Vastus	VAS	19187.90
Gluteus maximus	GMAX	6675.17
Hamstrings	HAMS	8210.93
Iliopsoas	ILPSO	5394.69
Rectus Femoris	RF	4383.48
Gastrocnemius	GAS	9381.15
Soleus	SOL	15849.99
Tibialis Anterior	TA	4233.64

**Table 1.** Muscles included in the model, their acronyms and their respective maximum isometric strengths (0% strength deficit).

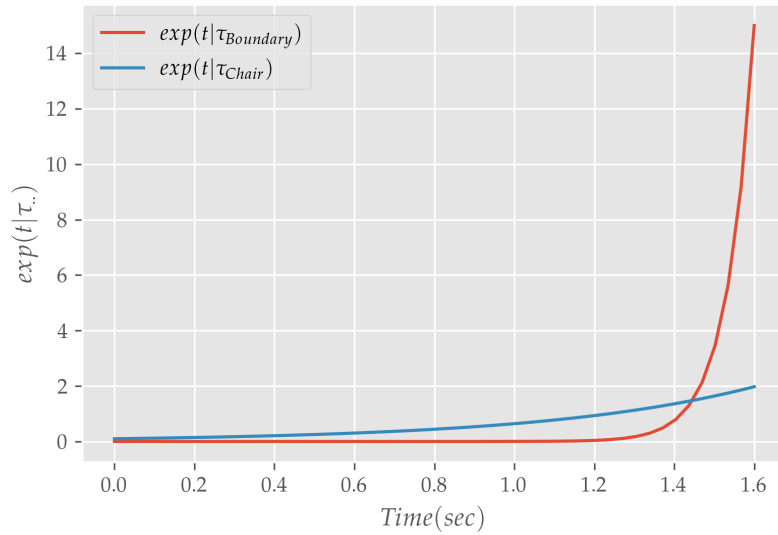


**Figure 3.**  $\exp(t|\tau_{..})$  for  $\tau_{Boundary}$ ,  $\tau_{Chair}$  and  $t_f = 1.6\text{sec}$

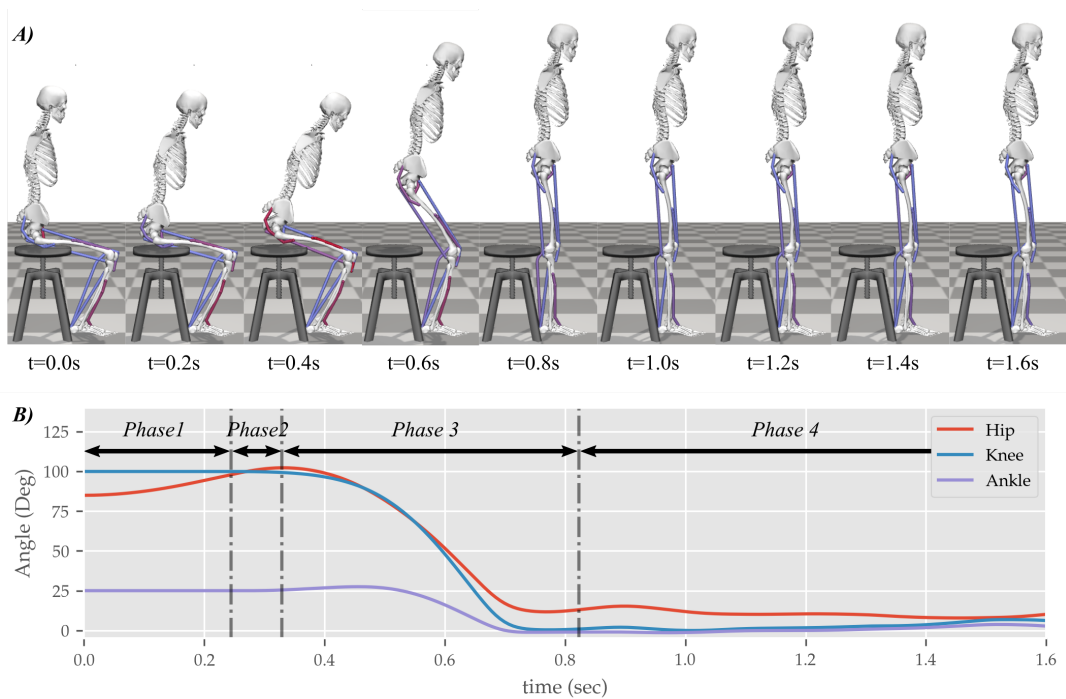


**Figure 4.** Postures (A) and joint angle trajectories (B) from the STS transition of 0% strength deficit model. In (A) the color gradient from blue to dark red represents the amount of muscle activation.

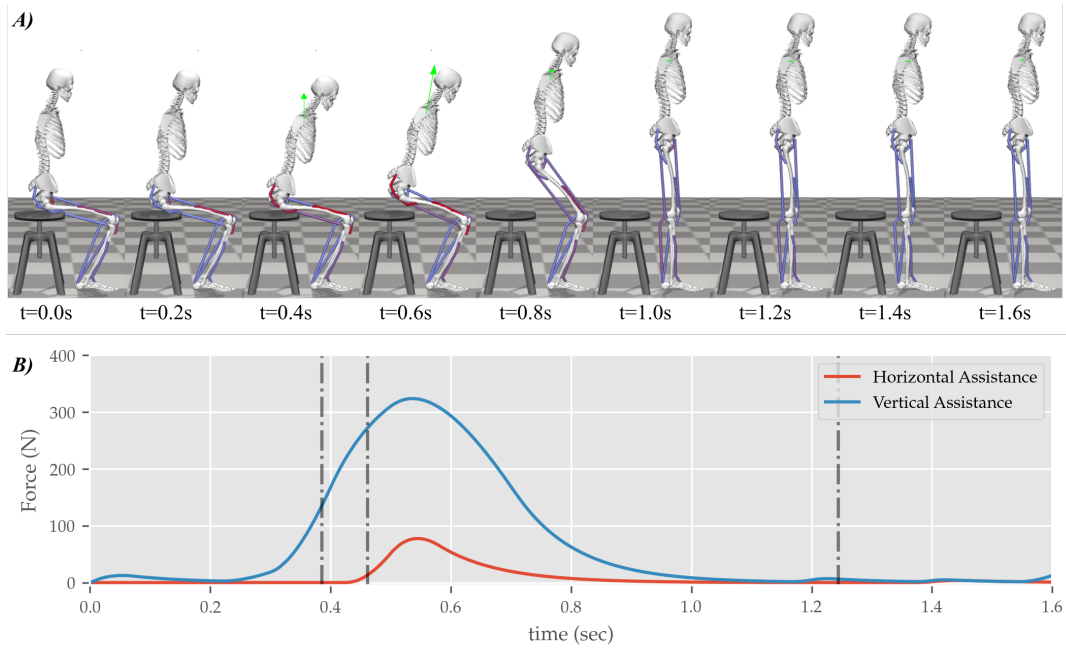


**Figure 5.** Postures (A) and the external assistance trajectories (B) from the STS transition of the externally assisted 60% strength deficit model. The green arrow in (A) represents the resultant external assistance force.

**Table 2.** List of cost function hyperparameter

Variable	Value
$\tau_{boundary}$	$t_f/24$
$\tau_{chair}$	$t_f/3$
$w_1$	800
$w_2$	600
$w_3$	0.4
$w_4$	100
$w_5$	20
$w_6$	0.2
$w_7$	10
$w_8$	0.1
$w_9$	20
$w_{10}$	0.1

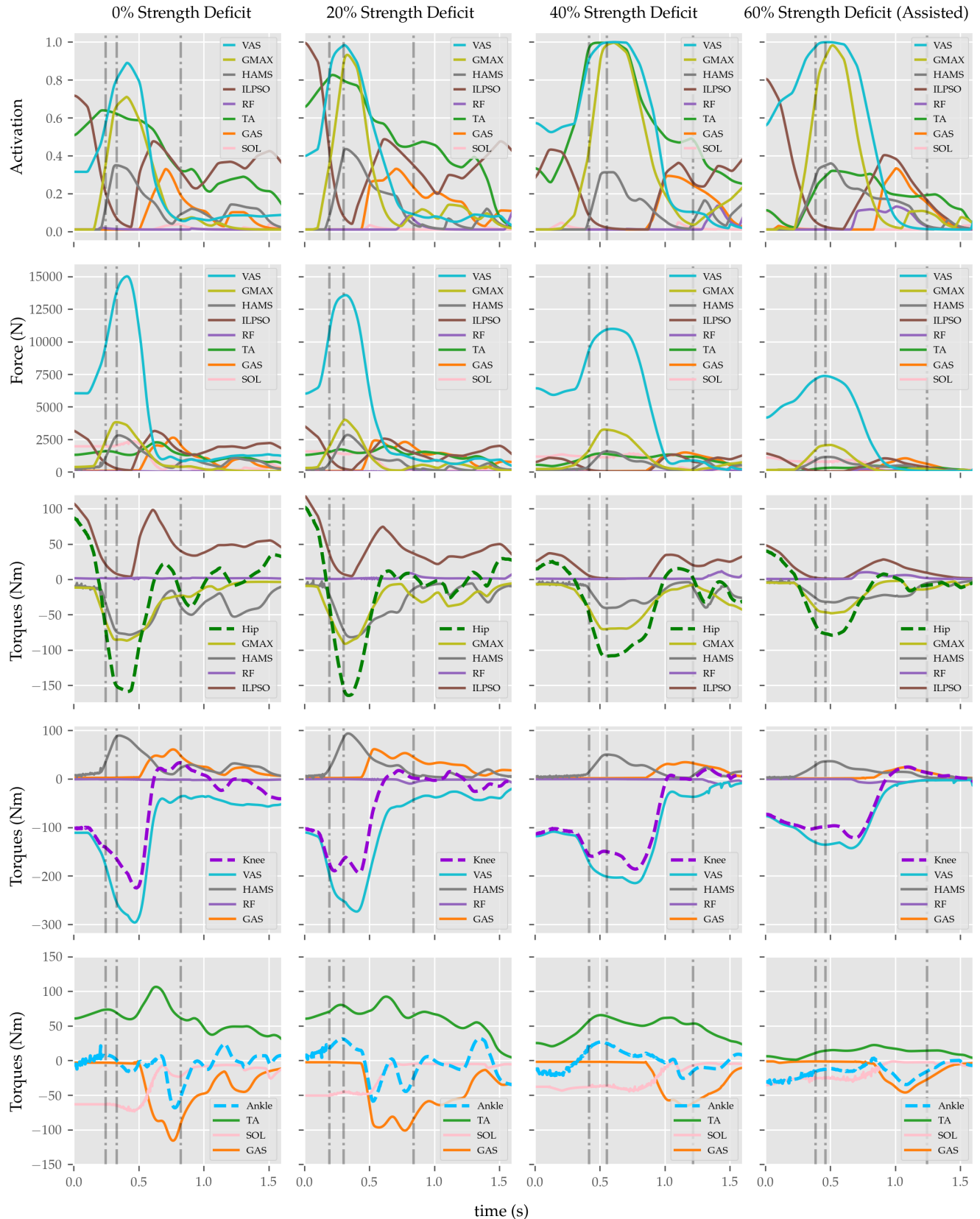


**Figure 6.** Muscle activations, muscle forces, and their respective contributions to the resultant joint torques from the STS trajectories of 0%, 20%, 40% and externally assisted 60% strength deficit models. The force and torque values correspond to the summation of respective values for the left and right legs.

**Table 3.** List of Symbols

Variable	Description
$t$	time
$t_0$	Start Time
$t_f$	Final Time
$\theta_j$	Angle of joint $j$
$..(t)$	Value of a expression .. at time $t$
$ .. $	The absolute value expression ..
$\tau$	time constant for $\exp()$ function
$y_{com}$	$y$ coordinate of COM
$x_{com}$	$x$ coordinate of COM
$x_{talus}$	$x$ coordinate of ankle
$F_{m,n}$	component of contact force acting on body $m$ in direction $n$
$a_m$	activation of muscle $m$
$\dot{a}_m$	rate of change of activation of muscle $m$
$\ F_{Assist}\ $	Magnitude of external assistance
$\text{bool}()$	boolean operation
$T_{n,limit}$	Torque generated by the torsional limit spring at the $n^{th}$ joint
$ZMP_x$	Horizontal component of feet force ZMP

**Table 4.** Properties from STS trajectories of the 0%, 20%, 40% and externally assisted 60% strength deficit models. Rows 4, 5, 7 and 9 shows contributions of muscles to peak resultant joint torques.

# Row	Property	0% Strength Deficit	20% Strength Deficit	40% Strength Deficit	Externally Assisted 60% Strength Deficit
1	STS duration (s)	0.82	0.84	1.22	1.24
2	Peak COM Vertical Velocity ( $m/s$ )	1.25	1.04	0.93	0.85
3	Peak Hip Torque ( $Nm$ )	-158.77	-164.32	-108.86	-79.06
4	GMAX Peak Hip Torque ( $Nm$ )	-86.46	-89.10	-70.30	-47.92
5	HAMS Peak Hip Torque ( $Nm$ )	-78.06	-81.30	-40.43	-32.51
6	Peak Knee Torque ( $Nm$ )	-224.96	-193.59	-186.01	-121.86
7	VAS Peak Knee Torque ( $Nm$ )	-294.04	-271.14	-214.99	-140.15
8	HAMS Peak Knee Torque ( $Nm$ )	67.03	75.76	27.75	20.51
9	Peak VAS Force ( $N$ )	15024.52	13573.82	10988.08	7372.93
10	Peak GMAX Force ( $N$ )	3826.64	4005.31	3256.65	2072.87
11	Peak HAMS Force ( $N$ )	2808.96	2842.76	1572.41	1150.42

## REFERENCES

- 367 Arnold, D. V. and Hansen, N. (2010). Active covariance matrix adaptation for the (1+ 1)-cma-es. In  
368     *Proceedings of the 12th annual conference on Genetic and evolutionary computation*. 385–392
- 369 Bobbert, M. F., Kistemaker, D. A., Vaz, M. A., and Ackermann, M. (2016). Searching for strategies to  
370     reduce the mechanical demands of the sit-to-stand task with a muscle-actuated optimal control model.  
371     *Clinical Biomechanics* 37, 83–90
- 372 Caruthers, E. J., Thompson, J. A., Chaudhari, A. M., Schmitt, L. C., Best, T. M., Saul, K. R., et al. (2016).  
373     Muscle forces and their contributions to vertical and horizontal acceleration of the center of mass during  
374     sit-to-stand transfer in young, healthy adults. *Journal of applied biomechanics* 32, 487–503
- 375 [Dataset] CMA-ES (2013). libcmaes. <https://github.com/CMA-ES/libcmaes>
- 376 Delp, S. L., Anderson, F. C., Arnold, A. S., Loan, P., Habib, A., John, C. T., et al. (2007). Opensim:  
377     open-source software to create and analyze dynamic simulations of movement. *IEEE transactions on*  
378     *biomedical engineering* 54, 1940–1950
- 379 Geravand, M., Korondi, P. Z., Werner, C., Hauer, K., and Peer, A. (2017). Human sit-to-stand transfer  
380     modeling towards intuitive and biologically-inspired robot assistance. *Autonomous Robots* 41, 575–592
- 381 Hughes, M. A., Myers, B. S., and Schenkman, M. L. (1996). The role of strength in rising from a chair in  
382     the functionally impaired elderly. *Journal of biomechanics* 29, 1509–1513
- 383 Lai, A. K., Arnold, A. S., and Wakeling, J. M. (2017). Why are antagonist muscles co-activated in my  
384     simulation? a musculoskeletal model for analysing human locomotor tasks. *Annals of biomedical*  
385     *engineering* 45, 2762–2774
- 386 Lord, S. R., Murray, S. M., Chapman, K., Munro, B., and Tiedemann, A. (2002). Sit-to-stand performance  
387     depends on sensation, speed, balance, and psychological status in addition to strength in older people.  
388     *The Journals of Gerontology Series A: Biological Sciences and Medical Sciences* 57, M539–M543
- 389 [Dataset] Millard, M. (1999). First-order activation dynamics
- 390 Millington, P. J., Myklebust, B. M., and Shambes, G. M. (1992). Biomechanical analysis of the sit-to-stand  
391     motion in elderly persons. *Archives of Physical Medicine and Rehabilitation* 73, 609–617
- 392 Mombaur, K. and Hoang, K.-L. H. (2017). How to best support sit to stand transfers of geriatric patients:  
393     Motion optimization under external forces for the design of physical assistive devices. *Journal of*  
394     *biomechanics* 58, 131–138
- 395 Ong, C. F., Geijtenbeek, T., Hicks, J. L., and Delp, S. L. (2019). Predicting gait adaptations due to ankle  
396     plantarflexor muscle weakness and contracture using physics-based musculoskeletal simulations. *PLoS*  
397     *computational biology* 15, e1006993
- 398 Pandy, M., Garner, B., and Anderson, F. (1995). Optimal control of non-ballistic muscular movements: a  
399     constraint-based performance criterion for rising from a chair. *Journal of Biomechanical Engineering*  
400     117, 15
- 401 Schenkman, M., Hughes, M. A., Samsa, G., and Studenski, S. (1996). The relative importance of strength  
402     and balance in chair rise by functionally impaired older individuals. *Journal of the American Geriatrics*  
403     *Society* 44, 1441–1446
- 404 Sherman, M. A., Seth, A., and Delp, S. L. (2013). What is a moment arm? calculating muscle effectiveness  
405     in biomechanical models using generalized coordinates. In *International Design Engineering Technical*  
406     *Conferences and Computers and Information in Engineering Conference* (American Society of  
407     Mechanical Engineers), vol. 55973, V07BT10A052
- 408 Yokota, H., Ohshima, S., and Mizuno, N. (2016). Sit-to-stand motion analysis using multiobjective  
409     genetic algorithm based on musculoskeletal model simulation. *IEEJ Journal of Industry Applications* 5,  
410     236–244